JTTEE5 19:1081–1092
DOI: 10.1007/s11666-010-9491-2
1059-9630/$19.00 © ASM International

Peer Reviewed

Effect of Powder Type and Composition on Structure and Mechanical Properties of Cu + Al_2O_3 Coatings Prepared by using Low-Pressure Cold Spray Process

Heli Koivuluoto and Petri Vuoristo

(Submitted December 28, 2009; in revised form February 4, 2010)

Powder type and composition have a very important role in the production of metallic and metallic-ceramic coatings by using the low-pressure cold spray process. Furthermore, structure and mechanical properties of Cu and Cu + Al_2O_3 coatings are strongly influenced by powder characteristics of Cu particles. The aim of this study was to evaluate the effect of different particle types of Cu powder and different compositions of added Al_2O_3 particles on the microstructure, fracture behavior, denseness, and mechanical properties, i.e., hardness and bond strength. Spherical and dendritic Cu particles were tested together with 0, 10, 30, and 50 vol.% Al_2O_3 additions. Coating denseness and particle deformation level increased with the hard particle addition. Furthermore, hardness and bond strength increased with increasing Al_2O_3 fractions. In the comparison between different powder types, spherical Cu particles led to the denser and less oxide-contenting coating structure due to the highly deformed particles.

Keywords Cu, Cu + Al_2O_3, low-pressure cold spraying, mechanical properties, structure

1. Introduction

Cold spraying is based on the utilization of significantly low process temperatures with high particle velocities. A coating is formed when powder particles impact at high velocities (above the material-dependent critical velocity) with high kinetic energy on the sprayed surface, deform and adhere to the substrate or to other particles (Ref 1, 2). Successful bonding between particles requires a high level of plastic deformation, adiabatic shear instabilities, and even more, material jets formation on the impacts (Ref 2-6). Typically, in the cold spray process, a gas is accelerated to supersonic velocity by a converging-diverging type nozzle (Ref 7). Cold spraying can be divided into two different processes: high-pressure (HPCS) and low-pressure cold spraying (LPCS). In LPCS, firstly, gas and powder are mixed in the diverging part of the nozzle from where particles are accelerated to the high-velocity particle-gas flow. Then after the exit of the nozzle, this particle-gas jet flows and impacts on the sprayed surface. The main differences between these two cold spray processes are the pressure level, 10 versus 40 bar, and type of powder injection, radial versus axial (Ref 8).

Heli Koivuluoto and **Petri Vuoristo**, Department of Materials Science, Tampere University of Technology, Tampere, Finland. Contact e-mail: heli.koivuluoto@tut.fi.

In LPCS, the preheating temperatures of the process gas are between room temperature and 650 °C, and pressures between 5 and 10 bar. Typically, in the low-pressure cold spray process, compressed air is used as the process gas to spray powder mixtures (Ref 9). Furthermore, particle velocities are reported to be in the range of 350-700 m/s in this spray process (Ref 10). Irissou et al. (Ref 11) have reported particle velocities for Al_2O_3 particles (mean size 25.5 μm) 580 m/s. In addition, Ning et al. (Ref 12) have presented mean particle velocities for Cu particles (30 μm) 450 m/s (sprayed with helium). Furthermore, irregular particles have reportedly higher in-flight velocities compared with spherical particles with the same particle sizes (Ref 12) due to the higher drag forces (Ref 13).

The LPCS is a relevant method to manufacture metallic coatings (e.g., Cu, Al, Ni, Zn, and Sn) with an addition of ceramic particles in the blended spray powder. There are three purposes for the use of hard ceramic particles in the powder mixtures. First, hard particles keep the nozzle clean and further, eliminate the nozzle clogging. Second, hard particles activate the sprayed surface by removing impurities, contamination, and oxide layers from the surface and additionally, roughening the surface. Third, hard particles reinforce the coating structure (Ref 14). Ceramic particles affect by the mechanical hammering of the substrate/sprayed layers or by the so-called shot peening via particle impacts (Ref 15). Furthermore, Shkodkin et al. (Ref 14) have reported increased bond strength and coating density with the increasing ceramic addition. Reportedly, the amount of ceramic particles in the sprayed coating structure is low in comparison with the initial powder composition. A hard

phase can be used to the purpose of reinforcement to strengthen the metallic matrix in LPCS process (Ref 16).

LPCS coatings similar with the HPCS coatings have highly deformed structure due to the high-velocity particle impacts. Plastic deformation level by the flattening of the sprayed metallic particles upon impacts is the relevant indicator to the quality of the coatings. Furthermore, the denseness and impermeability of the cold-sprayed coatings depend on the amount of deformation. High deformation levels lead to high denseness (Ref 5). Our previous study (Ref 17) showed microstructural details and existing through-porosity in the structure of LPCS $Cu + Al_2O_3$ coating. Additionally, powder characteristics are found to have the very crucial influence on coating formation and hence, coating properties in cold spraying (Ref 18, 19). Furthermore, suitable powders for cold spraying have specific particle size with narrow particle size distribution, depending on powder materials (Ref 18).

The aim of this study was to characterize Cu and $Cu + Al_2O_3$ coatings produced by using LPCS. Powder characteristics have a very important role in the coating and structure formation and thus, this study focuses on the characterization of LPCS Cu coatings sprayed from various feedstock material compositions. Furthermore, the effect of powder type (Cu) and composition ($Cu + Al_2O_3$) on structural details, e.g., microstructure and denseness, and mechanical properties were analyzed. Two different types of Cu powders are tested with four different compositions of added hard particles. Structural properties were evaluated using electron microscopy. In addition to these investigations, hardness and bond strength were measured in order to evaluate the mechanical behavior of the coatings.

2. Experimental Techniques

Two different Cu powders, a spherical and dendritic, were used as pure metallic powders with three different manually mixed compositions of Al_2O_3 particles. The production method of spherical particles was gas atomization whereas the dendritic particles got their morphologies by the electrolytic production method. In addition to these, a commercial powder mixture was tested as a reference. Table 1 summarizes powders and sample codes used. Morphologies of powders are presented in Fig. 1. Figure 1(a) shows the morphology of D_Cu powder, (b) added Al_2O_3 particles, (c) E_Cu dendritic Cu powder, and (d) O_Cu spherical Cu particles. All powders are commercially available. K-01-01 powder was supplied by Twin Trading Company (Moscow, Russia), and Ecka M15 by Ecka Granules (Furth, Germany), and Osprey Cu by Sandvik Osprey (Neath, UK). Oxygen content of E_Cu was $<0.15\%$ and of O_Cu it was 0.071% given by suppliers.

The LPCS Cu and $Cu + Al_2O_3$ coatings were prepared at Tampere University of Technology with the DYMET 304 K equipment (Obninsk Center for Powder Spraying, Obninsk, Russia). Compressed air was used as a process gas. Spraying parameters used are summarized in Table 2. The DYMET equipment was installed into an industrial robot. A round (∅ 5 mm) tubular nozzle was used. Substrates were grit-blasted (mesh 24, Al_2O_3 grits) Fe52 steel plates with the dimensions of 100 mm × 50 mm × 5 mm. In the bond strength tests, coatings sprayed with traverse speed of 7.4 m/min whereas in the other examinations, coatings sprayed with a traverse speed of 5 m/min were used. With O + 30 and O + 50 powders, feed rate was continuously regulated in order to gain smooth particle flow.

Powder morphologies were characterized using a Philips XL30 scanning electron microscope (SEM, Philips, Eindhoven, the Netherlands) whereas coating structures and fracture surfaces were characterized using a Zeiss ULTRAplus field-emission scanning electron microscope (FESEM, Carl Zeiss NTS GmbH, Oberkochen, Germany). The microstructures of LPCS coatings were studied from unetched metallographic cross-sectional samples. Denseness and particularly existing through-porosity (open-porosity/interconnected porosity) of the LPCS coatings were tested with corrosion tests; open-cell electrochemical potential measurements and salt spray tests. The electrochemical cell used in the open-cell potential measurements consisted of a tube, of diameter 20 mm and volume 12 mL, glued on the surface of the coating specimen. A 3.5 wt.% NaCl solution was put into the tubes for nine-day measurements. Open-cell potential measurements were done with a Fluke 79 III true RMS multimeter (Everett, WA). A silver/silver chloride (Ag/AgCl) electrode was used as a reference electrode. The salt spray test was done

Table 1 Powder characteristics of Cu and $Cu + Al_2O_3$ powders

Sample	Powder composition	Cu powder	Particle size of Cu powder, μm	Morphology of Cu powder	Amount of Al_2O_3, vol.%
D_Cu	$D\_Cu + Al_2O_3$	K-01-01	ca 15 (a)	Dendritic	~50 (a)
E_Cu	E_Cu	Ecka M15	<63	Dendritic	0
E + 10	$E\_Cu + 10Al_2O_3$	Ecka M15	<63	Dendritic	10
E + 30	$E\_Cu + 30Al_2O_3$	Ecka M15	<63	Dendritic	30
E + 50	$E\_Cu + 50Al_2O_3$	Ecka M15	<63	Dendritic	50
O_Cu	O_Cu	Osprey Cu	−25 + 5	Spherical	0
O + 10	$O\_Cu + 10Al_2O_3$	Osprey Cu	−25 + 5	Spherical	10
O + 30	$O\_Cu + 30Al_2O_3$	Osprey Cu	−25 + 5	Spherical	30
O + 50	$O\_Cu + 50Al_2O_3$	Osprey Cu	−25 + 5	Spherical	50

Particle sizes are given by producers
(a) With Dymet Cu powder particle size and amount of Al_2O_3 are visually analyzed from morphology images

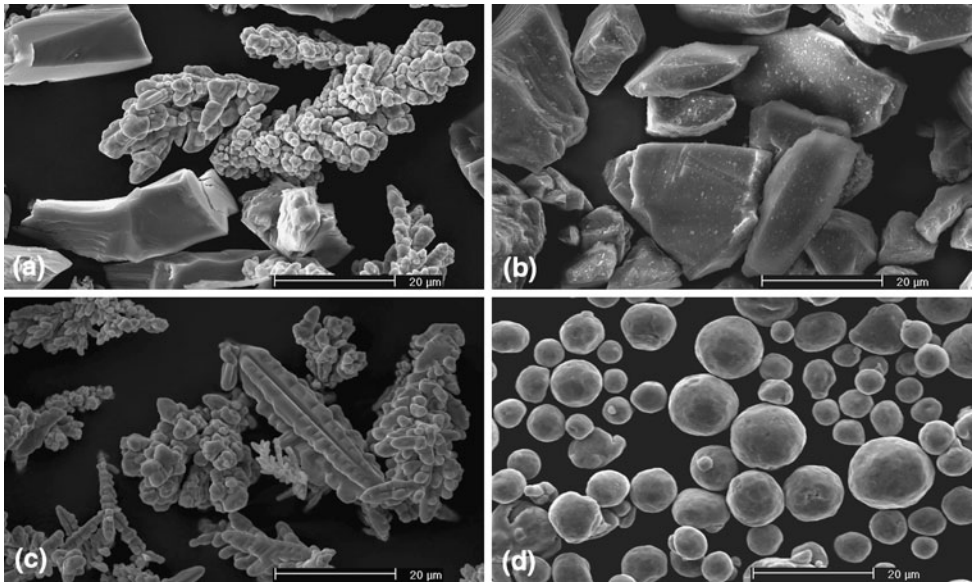

Fig. 1 Morphologies of (a) D_Cu, (b) Al_2O_3, (c) E_Cu, and (d) O_Cu powders. SEM images

Table 2 Spraying parameters of LPCS coatings

Spraying parameter	D_Cu	E_Cu, E + 10, E + 30, E + 50	O_Cu, O + 10	O + 30, O + 50
Pressure, bar	6	6	6	5
Preheating *T*, °C	540	540	540	540
Powder feed (equipment setting scale 1-8)	4.5	4.5	5.5	5-7 (a)
Traverse speed, m/min	5, 7.4	5, 7.4	5, 7.4	5, 7.4
Beam distance, mm	1	1	1	1
Spraying distance, mm	10	10	10	10
Number of layers	4	4	2	3

Beam distance stands for distance between two adjacent spray beads
(a) Powder feeding was continuously regulated

according to the ASTM B117 standard. A 5 wt.% NaCl solution was used with an exposure of 96 h, a temperature of 35-40 °C, a solution pH of 6.3, and a solution accumulation of 0.04 mL/cm^2 h. Coating surfaces after the salt spray test were visually analyzed. An amount of corrosion spots on the surfaces were evaluated by using image analysis program, ImageJ, which was also used in the analysis of Al_2O_3 fractions inside the coatings. Furthermore, mechanical properties were studied. Vickers hardness ($HV_{0.3}$) was measured as an average of 10 measurements with a Matsuzawa MMT-X7 hardness tester (Akita, Japan). Bond strength values were determined according to the standard EN582 in a tensile pull test (Instron 1185 mechanical testing machine, Norwood, MA). Three measurements were carried out to calculate the average values of bond strengths.

3. Results and Discussion

This study shows microstructural details using electron microscopic techniques, fracture surface analysis and denseness evaluations with corrosion tests. In addition to these, hardness and bond strength were investigated in order to find the relationship between the microstructure and the macroscopic properties of different LPCS Cu + Al_2O_3 mixture coatings.

3.1 Microstructures

The microstructural features of LPCS Cu + Al_2O_3 coating prepared from K-01-01 powder are presented in our previous study (Ref 17). This same powder was used also in the present study as a reference. Figure 2 shows cross-sectional structure (Fig. 2a) of D_Cu coating and interface between coating and grit-blasted steel substrate (Fig. 2b). Coating thickness was 276 μm (thickness of 1 layer 69 μm). Black particles are Al_2O_3 particles, arising from an initial powder mixture. The amount of Al_2O_3 particles inside the coating was 5.2% according to image analysis. Dendritic Cu particles were deformed on the impacts. However, some oxidized boundaries are observed in the microstructure as slightly darker gray areas between primary particles. Oxidized areas were caused by initial oxidized layers on the particle surfaces in the as-received

Peer Reviewed

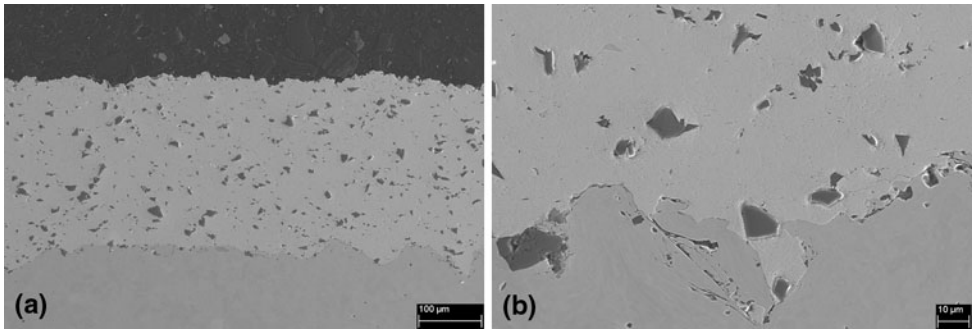

Fig. 2 Structure of D_Cu coating on grit-blasted steel substrate (a) general view and (b) interface between coating and substrate. FESEM images

state. Furthermore, dendritic particles had large surface areas due to the dendritic morphology of particles (Fig. 1c, powder particle consists of primary particles) and thus, high number of oxidized primary particle boundaries compared with spherical particles. An interface between coating and substrate was faultless and tightly adhered. Moreover, the interface seemed to be highly deformed (Fig. 2b).

Usually, hard particles are mixed with metallic particles in the LPCS process. There are three functions of use of ceramic particles: (i) cleaning the nozzle, (ii) activating the sprayed surface, and (iii) densifying the structure (Ref 17). In this study, pure Cu powders were also tested. The structure of E_Cu (dendritic) coating is presented in Fig. 3. The E_Cu coating contained some porosity and open boundaries in its structure concentrated mostly near to the coating surface. One reason for that could be that densifying effect of next incoming particles was missing and thus, coating had a porous layer on the top of the coating (Ref 20). Coating thickness was 258 µm (thickness of 1 layer 65 µm). In order to eliminate the porosity, Al_2O_3 particles were mixed with Cu powder.

The coating thicknesses increased with increasing amount of Al_2O_3 particles. The coating thicknesses of E + 10, E + 30, and E + 50 coatings were 328 µm (thickness of 1 layer 82 µm), 379 µm (thickness of 1 layer 95 µm), and 391 µm (thickness of 1 layer 98 µm), respectively. This indicates deposition efficiency improvement by using metallic-ceramic mixture powders. Figure 4 presents the structures of E + 10 (Fig. 4a) and E + 30 (Fig. 4b) coatings. These coatings contained also the porous layer near to the coating surface. However, the amount of porosity and open boundaries was decreased with the Al_2O_3 addition. This was due to the hammering effect of hard particles and thus, densification of the structure.

The strongest influence of hard particles on microstructure was detected with the highest amount of Al_2O_3 particles in the case of powder mixtures with dendritic Cu powder particles. The porous top layer was eliminated in the E + 50 coating which is seen in Fig. 5(a). Additionally, the detailed microstructure of E + 50 coating is presented in Fig. 5(b). Particle boundaries are partly seen in the structure, indicating that all oxide layers were not removed during particle impacts. In addition, very small-sized pores can be observed in the primary particle

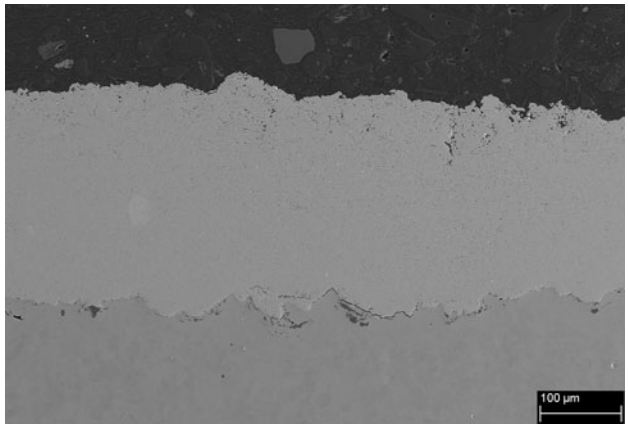

Fig. 3 Structure of E_Cu coating on grit-blasted steel substrate. FESEM image

boundaries. The dendritic particles were plastically deformed, but even higher deformation would be needed for eliminating all initial oxide layers of the powder particles. After removal of the oxide layers, it is possible to reveal the pure metallic surface and together with high contact pressure achieve the metallic bonding between primary Cu particles (Ref 6). However, the cross-sectional structure showed localized deformed grain structure inside the individual primary particles (Fig. 5b).

In addition to the dendritic Cu feedstock, the LPCS coatings were prepared from spherical Cu powders mixed with different amounts of Al_2O_3 particles. The structure of pure O_Cu (spherical) coating is presented in Fig. 6. The coating was mainly dense, containing only a few pores near to the coating surface. The porous layer was not received as well as in the coatings sprayed from dendritic Cu particles. It should be noticed that there is a lower amount of primary particle surfaces in the spherical, atomized particles arose from the higher primary particle size (ca 12.5 µm versus few microns) and thus, the higher volume of the individual primary particle (spherical powder particle versus dendritic primary particle in the powder particle), indicating possibility to have lower amount of oxidized particle boundaries. Additionally, oxide layers from initial Cu powder (direct reduction,

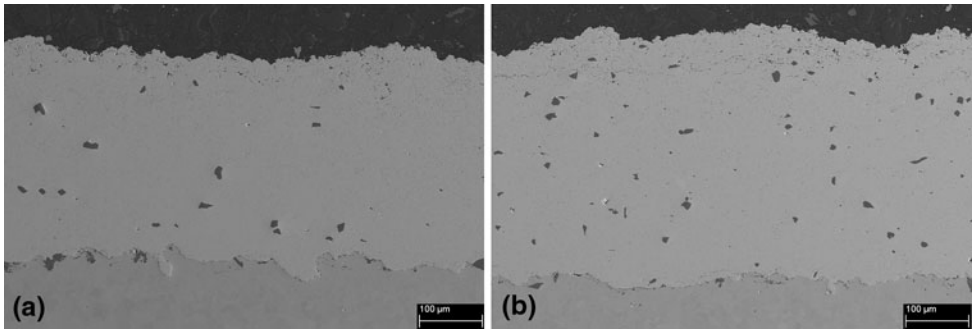

Fig. 4 Structures of (a) E + 10 and (b) E + 30 coatings on grit-blasted steel substrates. FESEM images

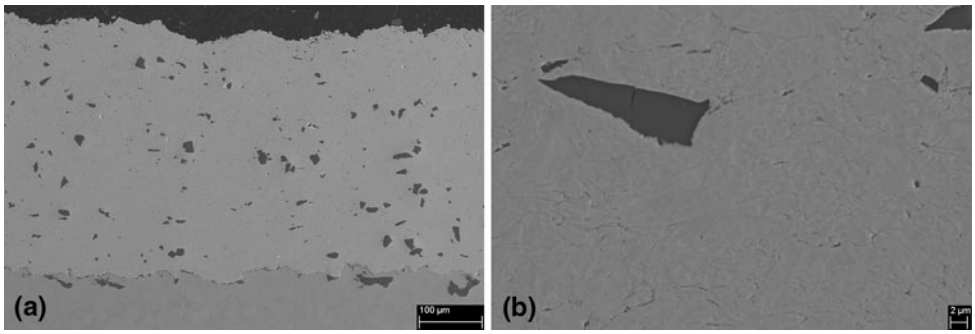

Fig. 5 Structure of E + 50 coating on grit-blasted steel substrate (a) general view and (b) detailed microstructure. FESEM images

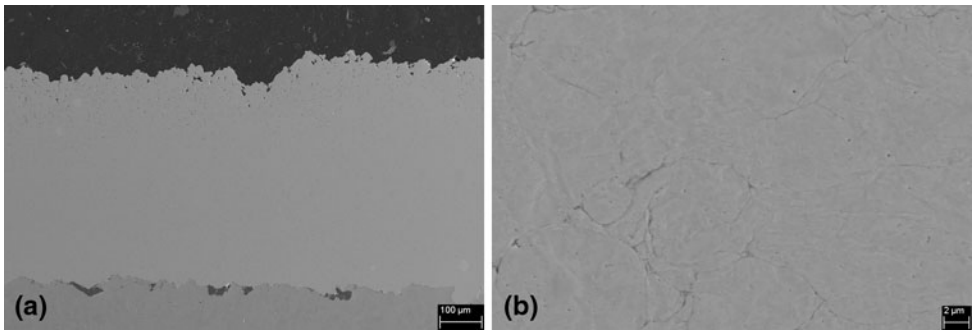

Fig. 6 Structure of O_Cu coating on grit-blasted steel substrate (a) general view and (b) detailed microstructure. FESEM images

convoluted particles) have reportedly incorporated as well in the HPCS Cu coating whereas the HPCS Cu coating sprayed from spherical powder was oxide-free (Ref 21). The coating thickness of O_Cu coating was 504 µm (thickness of 1 layer 252 µm). However, it should be noticed that coating thicknesses between coatings prepared from dendritic powder (Ecka M15) and spherical powder (Osprey) are not comparable because of different powder feed rates. The powder feed rate was continuously controlled in order to gain smooth powder flow in the case of O_Cu coatings. Figure 6(b) reveals the detailed microstructure of O_Cu coating. Oxidized particle boundaries, which were not removed during impacts, are detected inside the structure arose from initial oxide layers on the surfaces of the as-received powder particles as slightly darker gray boundaries in Fig. 6(b).

The structure of O + 10 coating is shown in Fig. 7. The coating had a relatively dense structure. Black particles inside the structure are Al_2O_3 particles arose from the powder mixture. The coating thickness was 441 µm (thickness of 1 layer 221 µm). More detailed structure is presented in Fig. 7(b). The addition of the hard particles was reinforced and hammered the structure and particles were undergone high plastic deformation. Therefore, more oxide layers were removed and metal-metal particle bonds were revealed. However, some oxidized boundaries

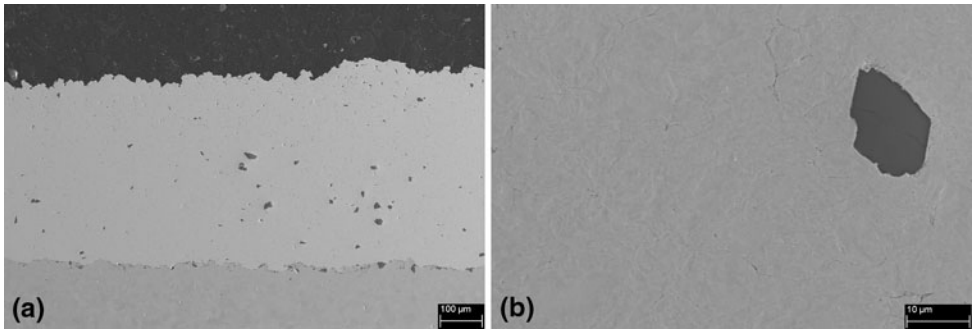

Fig. 7 Structure of O + 10 coating on grit-blasted steel substrate (a) general view and (b) detailed microstructure. FESEM images

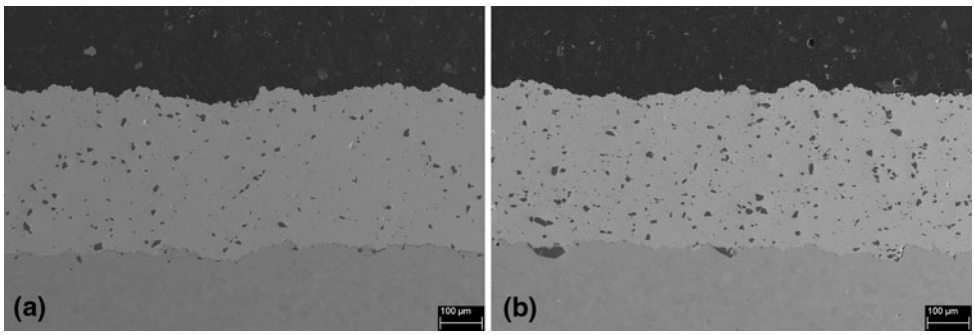

Fig. 8 Structure of (a) O + 30 and (b) O + 50 coatings on grit-blasted steel substrates. FESEM images

are still observed in the structure. In addition to the particle boundaries, localized grain deformation is detected in the interparticle structures.

Bonding between particles depends on powder materials, e.g., metallic and ceramic particles. In the optimal situation, metal-metal bonds are formed between metallic particles. Meanwhile, ceramic particles cannot be plastically deformed and hence, bonding mechanism between metallic and ceramic particles will be interlocking. The ceramic particles just stick to the metallic matrix. The amount of the hard particles has an effect on the coating formation of these composite coatings. In the case of spherical particles, the amount of 30% and 50% leads higher amount of Al_2O_3 particles to the coating structure. In turn, the higher amount of Al_2O_3 particles inside the coating possesses the higher amount of weaker ceramic-metallic bonds between particles. Bonding between metallic particles is stronger than between metallic and ceramic particles due to the bonding mechanisms (metal-metal bonds lead to the tighter adhesion between particles than sticking between metallic-ceramic particles). Figure 8 presents the structures of O + 30 (Fig. 8a) and O + 50 (Fig. 8b) coatings. The coating thicknesses were 370 µm (thickness of 1 layer 123 µm) and 364 µm (thickness of 1 layer 121 µm), respectively.

Al_2O_3 fractions were analyzed using image analysis and the amounts of Al_2O_3 particles inside the coating structures are presented in Table 3. Usually, coatings contain ceramic particles below 5% from total amount of ceramic powder, indicating erosion and on the other hand, activation occurred by ceramic particles (Ref 14, 22, 23). The similar behavior was also detected in this study.

Table 3 Amount of Al_2O_3 particles in the powder and inside the coating

Sample	Amount of Al_2O_3 particles in the powder, vol.%	Amount of Al_2O_3 particles inside the coating, %
D_Cu	~50	5.2
E_Cu	...	...
E + 10	10	0.9
E + 30	30	1.5
E + 50	50	3.6
O_Cu	...	...
O + 10	10	0.7
O + 30	30	2.0
O + 50	50	3.3

Amount inside the coating was done using image analysis (ImageJ)

Structures of LPCS Cu + Al_2O_3 coatings differed from each other, depending on sprayed feedstock. Obviously, coating sprayed with spherical Cu particles had larger primary particle size in the coating structure compared with the particle size of primary particles in the coating sprayed from dendritic Cu particles. The visually densest coating sprayed with dendritic powder (E_Cu) was achieved with the composition 50% Al_2O_3, whereas in the case of spherical Cu powder, the densest structure was gained with composition of 10% Al_2O_3 particles.

However, grain sizes are equal in these both coatings. The structure of LPCS $Cu + Al_2O_3$ coating prepared from spherical powder (O + 10) was denser and purer than the coating structure of E + 50 coating (compare Fig. 5b and Fig. 7b).

Spraying parameters have also influence on coating formation and deposition efficiency in LPCS process. Maev and Leshchynsky (Ref 4) have shown that deposition efficiency increased with the increasing preheating temperature of gas. Therefore, high preheating temperature (540 °C) of compressed air was used in this study. Additionally, this study is perceived the noticeable deposition efficiency increment with increasing amount of added Al_2O_3 particles with the dendritic Cu particles by comparison between coating thicknesses: 258 μm for E_Cu and 328-391 μm for $E + Al_2O_3$ coatings. Furthermore, the amount of Al_2O_3 particles in the coatings structures was obviously increased with increasing amount of hard particles in the powder mixture. Further, this trend was similar with spherical and dendritic Cu particles (Table 3).

3.2 Fracture Surfaces

Fracture surface analysis reveals particle deformation. Figure 9 presents the fracture surface of D_Cu coating. Localized deformation is detected in the structure (Fig. 9b). Powder particle boundaries are not clearly seen in the structure whereas primary particle boundaries are observed from the fracture surface. The blocky particles in Fig. 9 are Al_2O_3 particles which are embedded into the metallic structure. The coating structure prepared from dendritic feedstock contains high amount of primary particle boundaries and thus, probability to have oxidized boundaries is higher (Ref 17). In the other words, particles need to be deformed even higher level in order to get metal-metal bonding between Cu particles compared with the spherical Cu particles which have initially higher primary particle size and thus, lower amount of particle boundaries, and additionally, denser and purer particle structure in as-received state.

Figure 10 shows the fracture surface of Cu coating prepared from dendritic particles. The pure E_Cu coating is presented in Fig. 10(a) and E + 50 in Fig. 10(b). The densifying effect due to the more deformed particle structure with added hard particles (E + 50) is perceived from the structures. The primary particle boundaries are more clearly seen in the structure of E_Cu coating. The open particle boundaries were also detected in the microstructure of this coating (Fig. 3), indicating less deformed particles and hence, weak bonding between Cu particles. The primary Cu particles are strongly deformed in the coating structure with Al_2O_3 particles (Fig. 10b), reflecting the high effect of hard particles on the coating formation by increasing the deformation level of metallic particles.

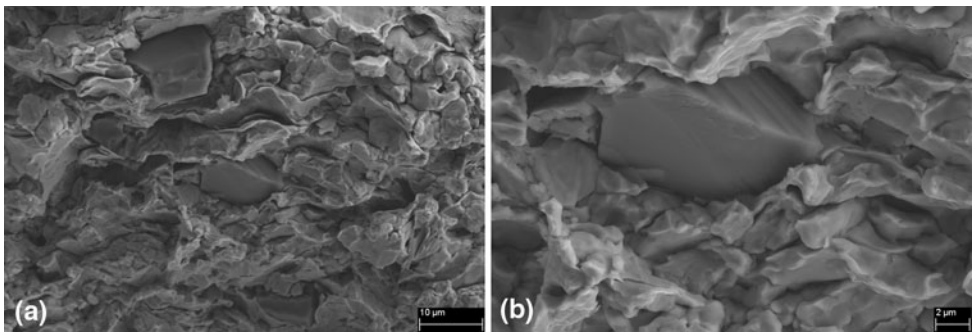

Fig. 9 Fracture surfaces of D_Cu coating (a) general and (b) detailed view. FESEM images

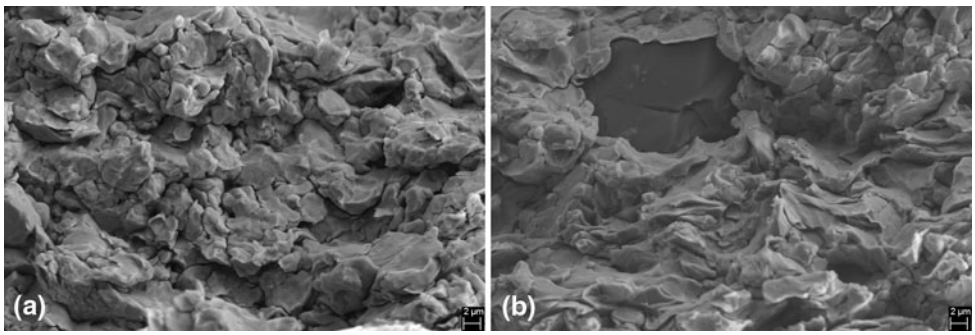

Fig. 10 Fracture surfaces of (a) E_Cu and (b) E + 50 coatings. FESEM images

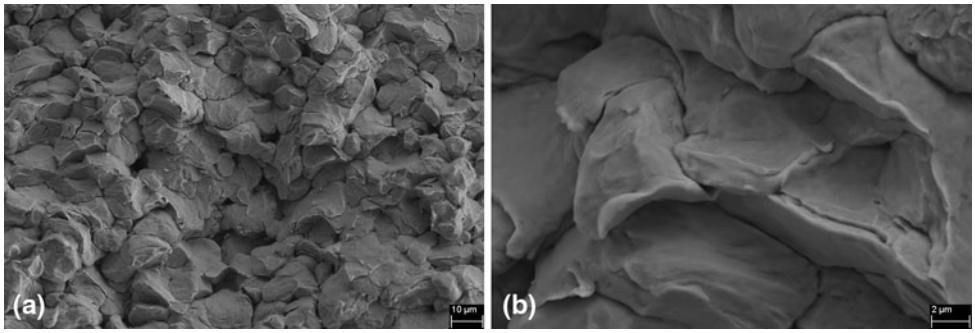

Fig. 11 Fracture surfaces of O_Cu coating (a) general and (b) detailed view. FESEM images

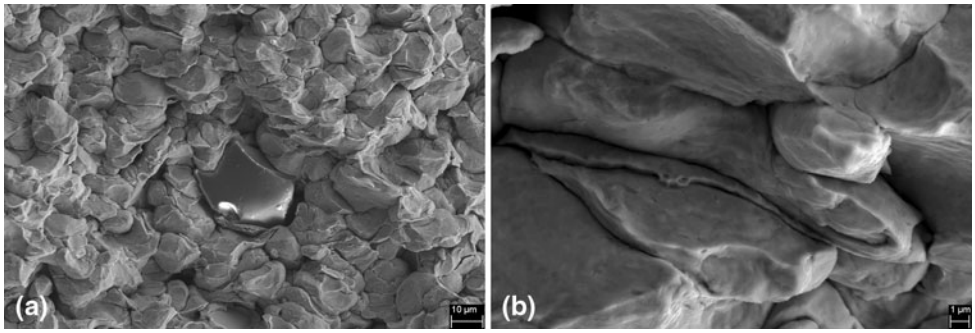

Fig. 12 Fracture surfaces of O + 10 coating (a) general and (b) detailed view. FESEM images

According to the salt spray test (in following "Denseness" section) and evaluation of microstructures, the densest coating prepared from spherical Cu particles was gained with 10% Al_2O_3 addition. In addition, the fracture surface of O + 10 showed tighter structure with higher deformation level compared with O_Cu coating without the ceramic addition. However, Cu particles in the O_Cu coating were also relatively highly deformed. Common for these both coatings and actually, also for D_Cu and E_Cu coatings, the fracture planes were mostly brittle type. The fracture surfaces of O_Cu and O + 10 coating are shown in Figs. 11 and 12, respectively. Figures 11(b) and 12(b) reveal high particle deformation as the flattened particle shapes. Additionally, material jets are observed inside the structure. Especially, in Fig. 12(b) narrow material jet is detected in the middle of the fracture surface. Formation of material jets is due to the thermal softening and adiabatic shear instability (Ref 6).

As a summary of the fracture surface analysis, particles were strongly deformed on the particle impacts. Moreover, Al_2O_3 addition hammered the structure, causing the higher level of plastic deformation occurrence and thus, highly deformed metallic structure. This was particularly seen with E + Al_2O_3 coatings. Particle bonds were tighter in the coatings prepared from spherical particles (O_Cu and O + Al_2O_3 coatings) compared with dendritic particles (D_Cu, E_Cu, and E + Al_2O_3 coatings). This was strongly influenced by the amount of particle boundaries. Larger primary particle size indicates denser coating structure arising from lower amount of particle boundaries as the weak points in the structure. On the other hand, material jets also clean the surfaces and promote metallic surfaces for the tight metal-metal bonding (Ref 6).

3.3 Denseness

Open-cell potential measurements showed existing through-porosity in all LPCS Cu coatings. The open-cell potentials of the LPCS Cu and Cu + Al_2O_3 coatings were between −519 and −610 mV, whereas open-cell potential of Fe52 substrate material was −700 mV. The open-cell potentials were close to the value of Fe52 substrate material, reflecting open way for test solution (3.5% NaCl) to penetrate from coating surface to the interface between coating and substrate. In addition, salt spray tests were gained as a supplementary evaluation. Existing through-porosity in the structure of coatings was also performed in the salt spray test. The amount of corrosion spots on the coating surfaces after the salt spray test was visually analyzed by using image analysis (ImageJ). Results are presented in Fig. 13. The amount of corrosion spots decreased with Al_2O_3 addition. The LPCS Cu coatings prepared from spherical feedstock had denser structure compared with the coatings prepared from dendritic feedstock. These results indicate that bonds between particles were tighter in these O_Cu coatings. Moreover, denseness was improved mostly with 10% Al_2O_3 addition to the O_Cu powder and 30% Al_2O_3 addition to the E_Cu

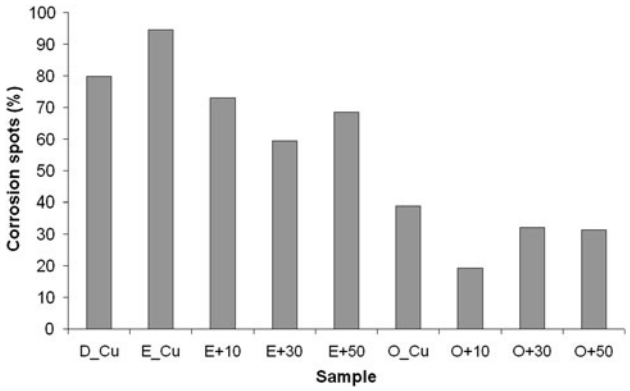

Fig. 13 Amount of corrosion spots (%) on coating surfaces after salt spray test analyzed by image analysis (ImageJ)

powder. The structure consisted mostly of metallic bonding have denser structure. However, low amount of added hard particles hammer the metallic structure, reinforcing the entire coating and thus, O + 10 coating had the highest denseness. Meanwhile, powder composed of dendritic Cu particles needed higher amount of hard particles to hammer the structure enough. On the other hand, amount of weaker bonds between metallic and ceramic particles than between metal-metal particles increases with higher amount of Al_2O_3 particles, reflecting to the denseness by again decreasing it. These different behaviors of dendritic and spherical mixture powders indicate clearly the importance of specific powder properties which should be chosen case by case.

Microstructural characterization together with corrosion tests clearly showed the effect of powder type of Cu particles and composition of added hard particles on coating formation and structure and therefore, also on the denseness (impermeability) of the coatings. The densest structures were achieved with coatings prepared from spherical powder particles (O_Cu and O + Al_2O_3 coatings). This was affected by the density of the powder particle and the number of primary particle boundaries (oxidized boundaries). Therefore, lower number of particle boundaries with lower number of oxidized particle surfaces generates tighter structure and thus, the higher denseness of the coating. With the spherical particle mixtures, the effect of hard particles was not as high as in the case of dendritic particles. The highest denseness of O_Cu coatings was detected with 10% Al_2O_3 particle addition into the initial powder mixture. In the case of dendritic particles, the highest denseness was gained with 30% and 50% Al_2O_3 addition. In conclusion, salt spray tests showed that all coatings tested in this study contained through-porosity in their structure. However, denseness improvement was clearly observed with Al_2O_3 additions, reflecting their significant effect on coating formation.

3.4 Hardness

Vickers hardness was measured in order to evaluate differences in the mechanical properties of coatings prepared from different-type powder characteristics. Hardness indicates level of work hardening. Table 4 summarizes Vickers hardness $HV_{0.3}$ of LPCS coatings. LPCS Cu coating sprayed with dendritic feedstock powder particles (E_Cu) have lower hardness than coating sprayed with spherical particles (O_Cu). McCune et al. (Ref 21) have reported similar behavior where the HPCS Cu coating sprayed from spherical (gas-atomization) Cu particles possessed higher hardness compared with coating sprayed from convoluted (direct reduction) Cu particles. Furthermore, hardness increases with increasing Al_2O_3 addition, indicating the high deformation and thus, the higher hardening effect. It should be noticed that indentation was taken from metallic area of the coating in order to analyze the behavior of metallic Cu particles. In addition, if we compare Cu + 50Al_2O_3 coatings, it can be noticed that O + 50 coating had the highest hardness, then D_Cu coating and after that E + 50 coating had the lowest hardness in this comparison. The trend in the hardness values was comparable to the microscopic evaluations, reflecting the strong effect of powder type and composition on the deformation, denseness, particle bonding, and work hardening.

Table 4 Vickers hardness $HV_{0.3}$ of LPCS Cu and Cu + Al_2O_3 coatings

Sample	Vickers hardness $HV_{0.3}$	SD
D_Cu	117	3.4
E_Cu	83	3.9
E + 10	95	7.6
E + 30	96	4.3
E + 50	103	4.6
O_Cu	106	6.0
O + 10	113	4.1
O + 30	127	3.3
O + 50	127	8.9

3.5 Bond Strength

The bond strength of LPCS Cu coating prepared from dendritic powder (K-01-01) was cohesive type in our previous study (Ref 17). In this study, the bond strength of D_Cu coating which was prepared from the same powder as feedstock showed also cohesive type bond strength. On the contrary, in the cases of E_Cu and E + Al_2O_3 coatings samples fractured partly from the coating-substrate interface and partly close to the interface in the coating side. However, it can be said that bond strength was mostly adhesive type because the rupture was still occurred mostly at the interface. In the case of O_Cu and O + Al_2O_3 coatings, bond strength was clearly adhesive type due to the fact that the weakest point in the tensile test was the interface between coating substrate. The adhesive rupture and thus, the adhesive-type bond strength in both cases, O_Cu and E_Cu coatings mixed with Al_2O_3 particles was possibly due to the hammering effect of Al_2O_3 particles. The Al_2O_3 particles tamped the coating structure, leading higher cohesion between particles compared with adhesion between coating and

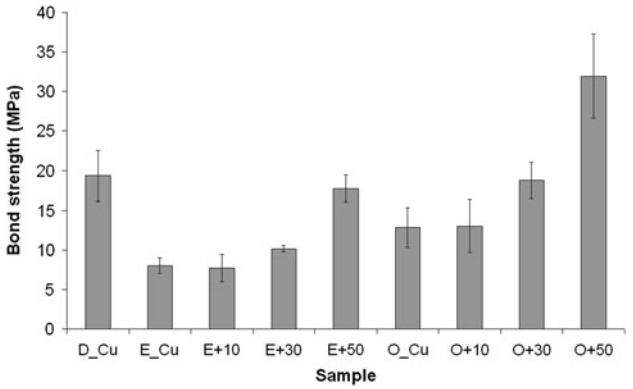

Fig. 14 Bond strengths (and standard deviations) of LPCS Cu and Cu + Al_2O_3 coatings. D_Cu coating had cohesive type, E_Cu and E + Al_2O_3 coatings mostly adhesive type, and O_Cu and O + Al_2O_3 coatings adhesive-type bond strengths

substrate. Bonds between Al_2O_3 and Cu particles were weaker than bonds between the metallic particles (sticking versus metallic bonding). Thus, it is more probable that fracture occurs inside the D_Cu coating where the amount of Al_2O_3 particles was higher and bonds between particles weaker. Besides, the lower amount of hard particles inside the coating (compare D_Cu coating with E + 50 and O + 50 coatings) indicates more bonding areas between the metallic particles. Figure 14 summarizes the bond strengths of the coatings. It can be clearly seen that the bond strengths increase with the increasing amount of Al_2O_3 particles in the initial manually mixed powder mixtures. This effect was also detected in Ref 14, 24, and 25. In addition, coatings prepared from spherical particles (O_Cu and O + Al_2O_3) had the higher bond strengths caused by higher plastic deformation together with more oxidized-free particle boundaries (purer coatings). Maev and Leshchynsky (Ref 8) have reported the adhesion strength of Cu-based coating on steel substrate ~27 MPa which is comparable with results in this study.

Generally speaking, the bond strengths of the LPCS coatings are reasonable. However, bonding and as well as bond strengths are strongly influenced by powder characteristics and compositions. Regardless of the powder characteristics of Cu particles, the bond strength of the LPCS Cu coatings depends on the amount of Al_2O_3 particles in the powder mixtures. This study showed that bond strength was the highest with 50% Al_2O_3 addition. This was due to the activation effect of hard particles (also hammering and tamping effects) together with increased contact areas (Ref 24) on the substrate surfaces. Bonding between grit-blasted steel substrate and powder particles was stronger, reflecting higher plastic deformation occurred on the impacts. Moreover, higher deformation level was also detected in the microscopic evaluations. Spherical particles underwent higher plastic deformation (lower content of oxidized primary particle boundaries) and hence, also the bond strengths of the coatings prepared from spherical particles (Osprey) are relatively higher than in the case of the coating prepared from dendritic particles (K-01-01 and Ecka). This was clearly observed in both O_Cu and E_Cu mixture coatings with all powder composition (0%, 10%, 30%, and 50% Al_2O_3 addition).

4. Conclusions

The LPCS process is the relevant method to prepare Cu and Cu + Al_2O_3 coatings. These coatings were relatively dense according to visual examination. However, corrosion tests revealed through-porosity inside the coating structures. Moreover, powder characteristics and compositions affected the denseness and mechanical properties of the coatings. In this study, the effect of powder type, i.e., dendritic versus spherical Cu particles, and the amount of Al_2O_3 particles in the powder mixtures were characterized. The study was focused on the microstructural details and mechanical behavior of the LPCS Cu coatings manufactured by using different feedstock.

The LPCS Cu and Cu + Al_2O_3 coatings prepared from the spherical Cu particles contained less through-porosity in their structures compared with coatings prepared from the dendritic particles, indicating denser coating structures. It was possible to produce pure Cu coatings from both spherical and dendritic feedstock by using LPCS process; however, the quality of the coatings can be improved with the hard particle additions. This study has clearly shown that more deformed and denser coating structure together with higher hardness and bond strength were gained with Al_2O_3 particle addition into the Cu powder. Densification was noticeable with the E + Al_2O_3 coatings (dendritic Cu particles) and according to corrosion tests; the densest structure was achieved with the amount of 30% Al_2O_3 particles. Porosity was significantly diminished with increasing amount of Al_2O_3 particles in the initial powder mixture. In addition to that, fracture surface analysis showed much higher level of deformation of Cu particles when Al_2O_3 particles were mixed with Cu particles, reflecting the densifying and hammering effect of hard particles.

On the other hand, O_Cu and O + Al_2O_3 coatings had denser structures than E_Cu and E + Al_2O_3 coatings. This can be explained by the powder characteristics; particle morphologies, primary particle sizes and purity of the initial powder particles. Usually, if the coating has weak points in its structure, they are detected on the particle boundaries and because of that affect particle bonding. The dendritic particles have more boundaries in the structure due to the finer particle size of primary particles and thus, more possibilities to have weak bonds between the particles due to the higher amount of oxidized particle boundaries. The O + 10 coating had the densest structure according to the microscopic evaluation and in addition to that, the corrosion tests. Meanwhile, the O + 50 coatings had the highest hardness and bond strength. Firstly, the higher amount of Al_2O_3 particles causes the higher level of work hardening which is reflected on the hardness values. On the other hand, bond strengths (adhesive

strength, fracture surface was between coating and substrate) were higher due to the stronger activation effect of Al_2O_3 particles on substrate surface by increasing and cleaning the contact areas. Second, metallic bonding makes the structure denser and thus, 10% Al_2O_3 addition forms denser structure than 50% addition and thus, 10% was enough to hammer the structure.

The hardnesses and bond strengths of the coatings were strongly depended on the powders used. The hardness and bond strength were increased with the increasing amount of hard particles in both cases of LPCS Cu mixture coatings prepared from either spherical or dendritic feedstock. However, it should be noticed that the hardness and bond strengths were higher when using the spherical Cu particles compared with the dendritic particles. Denser powder particles with higher primary particle size can be explained this effect due to the fact that spherical particles underwent the higher level of plastic deformation. Thus, they have probability to have the lower number of weak particle boundaries.

This study presented the effect of powder characteristics on the coating properties. Densification was significantly detected, but still LPCS Cu and $Cu + Al_2O_3$ coatings contained through-porosity. However, this study has clearly shown the importance of the powders in the cold spraying and shown the possibility to improve coating quality by using the metallic-ceramic mixture powders with optimized characteristics together with optimized compositions, depending on the coating properties desired.

Acknowledgments

The authors thank Mr. Mikko Kylmälahti, of Tampere University of Technology, Department of Materials Science, for the spraying the LPCS coatings and Mr. Sakari Tolvanen of Tampere University of Technology, Department of Materials Science for the carrying out the bond strength tests. In addition, the authors express thanks to Mr. Jonne Näkki of KETEK for the salt spray tests. This study was supported by Academy of Finland and Finnish National Graduate School on New Materials and Processes.

References

1. A. Papyrin, V. Kosarev, S. Klinkov, A. Alkimov, and V. Fomin, 2007, *Cold Spray Technology*, 1st ed., Elsevier, the Netherlands, 328 p
2. T. Schmidt, F. Gärtner, H. Assadi, and H. Kreye, Development of a Generalized Parameter Window for Cold Spray Deposition, *Acta Mater.*, 2006, **54**(3), p 729-742
3. C. Borchers, F. Gärtner, T. Stoltenhoff, H. Assadi, and H. Kreye, Microstructural and Macroscopic Properties of Cold Sprayed Copper Coatings, *J. Appl. Phys.*, 2003, **93**(12), p 10064-10070
4. R. Maev and V. Leshchynsky, Air Gas Dynamic Spraying of Powder Mixtures: Theory and Application, *J. Therm. Spray Technol.*, 2006, **15**(2), p 198-205
5. H. Assadi, F. Gärtner, T. Stoltenhoff, and H. Kreye, Bonding Mechanism in Cold Gas Spraying, *Acta Mater.*, 2003, **51**, p 4379-4394
6. M. Grujicic, C.L. Zhao, W. DeRosset, and D. Helfritch, Adiabatic Shear Instability Based Mechanism for Particles/Substrate Bonding in the Cold-Gas Dynamic-Spray Process, *Mater. Design*, 2004, **25**, p 681-688
7. T. Stoltenhoff, H. Kreye, and H. Richter, An Analysis of the Cold Spray Process and Its Coatings, *J. Therm. Spray Technol.*, 2001, **11**(4), p 542-550
8. R. Maev and V. Leshchynsky, *Introduction to Low Pressure Gas Dynamic Spray, Physics & Technology*, Wiley-VCH Verlag GmbH&Co, KGaA, Weinheim, Germany, 2008, p 328
9. A. Kashirin, O. Klyuev, T. Buzdygar, and A. Shkodkin, DYMET Technology Evolution and Application, *Thermal Spray 2007: Global Coating Solutions*, B. Marple, M. Hyland, Y. Lau, C.-J. Li, R. Lima, and G. Montavon, Ed., May 14-16, 2007 (Beijing, China), ASM International, 2007, p 141-145
10. X.-J. Ning, J.-H. Jang, H.-J. Kim, C.-J. Li, and C. Lee, Cold Spraying of Al-Sn Binary Alloy: Coating Characteristics and Particle Bonding Features, *Surf. Coat. Technol.*, 2008, **202**(9), p 1681-1687
11. E. Irissou, J.-G. Legoux, B. Arsenault, and C. Moreau, Investigation of Al-Al_2O_3 Cold Spray Coating Formation and Properties, *J. Therm. Spray Technol.*, 2007, **16**(5-6), p 661-668
12. X.-J. Ning, J.-H. Jang, and H.-J. Kim, The Effects of Powder Properties on In-Flight Particle Velocity and Deposition Process During Low Pressure Cold Spray Process, *Appl. Surf. Sci.*, 2007, **253**(18), p 7449-7455
13. B. Jodoin, L. Ajdelsztajn, E. Sansoucy, A. Zúñiga, P. Richter, and E. Lavernia, Effect of Particle Size, Morphology, and Hardness on Cold Gas Dynamic Sprayed Aluminum Alloy Coatings, *Surf. Coat. Technol.*, 2006, **201**, p 3422-3429
14. A. Shkodkin, A. Kashirin, O. Klyuev, and T. Buzdygar, The Basic Principles of DYMET Technology, *Thermal Spray 2006: Building on 100 Years of Success*, B. Marple, M. Hyland, Y. Lau, R. Lima, J. Voyer, Ed., May 15-18, 2006 (Seattle, Washington), ASM International, 2006
15. B. Djordjevic, and R. Maev, SIMAT™ Application for Aerospace Corrosion Protection and Structural Repair, *Thermal Spray 2006: Building on 100 Years of Success*, B. Marple, M. Hyland, Y. Lau, R. Lima, J. Voyer, Ed., May 15-18, 2006 (Seattle, Washington), ASM International, 2006
16. H. Weinert, E. Maeva, and E. Leshchynsky, Low Pressure Gas Dynamic Spray Forming Near-net Shape Parts, *Thermal Spray 2006: Building on 100 Years of Success*, B. Marple, M. Hyland, Y. Lau, R. Lima, and J. Voyer, Ed., May 15-18, 2006 (Seattle, Washington), ASM International, 2006
17. H. Koivuluoto, J. Lagerbom, M. Kylmälahti, and P. Vuoristo, Microstructure and Mechanical Properties of Low-Pressure Cold Sprayed (LPCS) Coatings, *J. Therm. Spray Technol.*, 2008, **17**(5-6), p 721-727
18. V. Champagne, Ed., *The Cold Spray Materials Deposition Process: Fundamentals and Applications*, Woodhead Publishing Limited, Cambridge, England, 2007, p 362
19. H. Mäkinen (Koivuluoto), J. Lagerbom, and P. Vuoristo, Adhesion of Cold Sprayed Coatings: Effect of Powder, Substrate, and Heat Treatment, *Thermal Spray 2007: Global Coating Solutions*, B. Marple, M. Hyland, Y.-C. Lau, C.-J. Li, R. Lima, and G. Montavon, Ed., May 14-16, 2007 (Beijing, China), ASM International, 2007, p 31-36
20. H. Mäkinen (Koivuluoto), J. Lagerbom, and P. Vuoristo, Mechanical Properties and Corrosion Resistance of Cold Sprayed Coatings, *Thermal Spray 2006: Building on 100 Years of Success*, B. Marple, M. Hyland, Y. Lau, R. Lima, and J. Voyer, Ed., May 15-18, 2006 (Seattle, Washington), ASM International, 2006
21. R.C. McCune, W.T. Donlon, O.O. Popoola, and E.L. Cartwright, Characterization of Copper Layers Produced by Cold Gas-Dynamic Spraying, *J. Therm. Spray Technol.*, 2000, **9**(1), p 73-82
22. A. Shkodkin, A. Kashirin, O. Klyuev, and T. Buzdygar, Metal Particle Deposition Stimulation by Surface Abrasive Treatment in Gas Dynamic Spraying, *J. Therm. Spray Technol.*, 2006, **15**(3), p 382-386

23. S.V. Klinkov, V.F. Kosarev, A.A. Sova, and I. Smurov, Calculation of Particle Parameters for Cold Spraying of Metal-Ceramic Mixtures, *J. Therm. Spray Technol.*, 2009, **18**(5-6), p 944-956
24. H.Y. Lee, S.H. Jung, S.Y. Lee, Y.H. You, and K.H. Ko, Correlation Between Al_2O_3 Particles and Interface of Al-Al_2O_3 Coatings by Cold Spray, *Appl. Surf. Sci.*, 2005, **252**, p 1891-1898
25. K. Spencer, D.M. Fabijanic, and M.-X. Zhang, The Use of Al-Al_2O_3 Cold Spray Coatings to Improve the Surface Properties of Magnesium Alloys, *Surf. Coat. Technol.*, 2009, **204**, p 336-344